Spectrum of Engineering Sciences
ISSN (e) 3007-3138 (p) 3007-312X
Volume 4, Issue 2, 2026

OBSERVER-BASED SLIDING MODE APPROACH FOR SYNCHRONIZING MOTION IN LARGE AIRCRAFT HYBRID MECHATRONIC ACTUATION SYSTEM

Waheed Ur Rehman[*1,2], Zeeshan Hameed[3], Mohsin Mumtaz Tarar[4], Muhammad Shoaib[5], Jamshed Ali[6], Attiq-Ur-Rehman[7], Muhammad Arqum Razzaq[8]

[*1]*School of Automation Science and Electrical Engineering, Beihang University, Beijing 100191, China*
[2]*Department of Mechatronics Engineering, University of Chakwal, Chakwal 48800, Pakistan*
[3]*Free University of Bozen-Bolzano, Bolzano, 39100, Italy*
[4]*Department of Electronics Engineering, University of Chakwal, Chakwal 48800, Pakistan*
[5]*School of business Administration, Zhejiang Gongshang University Hangzhou,China*
[6]*Faculty of Engineering / School of Computer Science and Engineering, South China University of Technology, China*
[7]*Department of Economics & Agricultural Economics, Pir Mehr Ali Shah, Arid Agriculture University, Rawalpindi*
[8]*Department of Mechatronics Engineering, University of Chakwal, Chakwal 48800, Pakistan*

[*1]wrehman87@buaa.edu.cn, [2]waheed.urrehman@uoc.edu.pk, [3]Zeeshan.Hameed@unibz.it, [4]mohsin.tarar@uoc.edu.pk, [5]shoaibch.127@gmail.com, [6]shaikhjamashedali@scut.edu.cn, [7]ateeeeqmaliks@gmail.com, [8]arqum.razzaq@uoc.edu.pk

DOI: https://doi.org/10.5281/zenodo.18591363

Keywords
Sliding Mode Control; Motion Synchronization; Hybrid mechatronics actuation system, Electro mechanical Actuator; Servo Hydraulic actuators; Extended state observer

Article History
Received: 11 December 2025
Accepted: 26 January 2026
Published: 10 February 2026

Corresponding Author: * Waheed Ur Rehman

Abstract

*In hybrid mechatronic actuation systems comprising electro-mechanical and servo-hydraulic actuators, precise motion synchronization is imperative for reliable performance, particularly in large-scale civil aircraft applications. A lack of synchronization between actuators gives rise to the *Force-Fighting* phenomenon, which occurs when differential forces are produced while both actuators jointly drive the same control surface. This research investigates the mitigation of Force-Fighting and the enhancement of motion coordination within hybrid actuation systems. An observer-based Sliding Mode Control (SMC) framework is proposed to achieve robust motion synchronization. To address modeling uncertainties, actuator coupling effects, external disturbances, and the unavailability of complete state information, an Extended State Observer (ESO) is integrated into the control design. The effectiveness of the proposed scheme is validated through extensive simulations conducted in MATLAB/Simulink. Comparative results with existing methods demonstrate that the proposed control approach significantly improves motion synchronization accuracy, enhances load disturbance rejection capability, and effectively suppresses the Force-Fighting phenomenon in hybrid mechatronic actuation systems.*

1. Introduction

In contemporary studies on aircraft control systems, actuator malfunction represents a significant area of concern [1-4]. In recent years, considerable research has been conducted to identify potential issues that may arise in aerospace vehicle systems. Moreover, several researchers have emphasized the role of safety and explored artificial intelligence techniques to mitigate these challenges [5, 6]. To achieve higher levels of reliability and safety, modern aircraft have

adopted hybrid mechatronic actuation systems within their primary control structures. The Airbus A320, for instance, uses such systems to manage the elevator, rudder, and aileron functions [7]. In aircraft control systems, actuators are indispensable elements that control the motion and dynamics of the flight surfaces [8]. Historically, aircraft control surfaces were driven solely by hydraulically powered actuators. Over time, ensuring the safety and reliability of flight control systems became a central concern. To address these aspects, redundant actuation configurations were introduced as the aviation industry evolved. However, it was later observed that when common-mode or common-cause failures occur within these redundant systems, safety risks persist. Such limitations have consequently restricted further improvements in the reliability and safety of redundant actuation architectures [9, 10]. Further progress in redundant actuation system studies led to the inclusion of an electromechanical actuator in addition to the hydraulic actuator. This integration aims to mitigate common-mode and common-cause failures while improving the reliability and safety of redundant actuation systems within the aerospace industry [11, 12].

Ongoing research developments have resulted in the design of a hybrid actuation configuration, termed the Hybrid Mechatronic Actuation System (HAS), consisting of both Electromechanical Actuators (EMA) and Electro-Hydraulic Servo Actuators (SHA). The combination of these technologies considerably strengthens the safety and dependability of the aircraft's control actuation mechanisms [13]. Advancements in the study of More Electric Aircraft have contributed to enhanced reliability by incorporating electrical generation units, power electronics, actuators, electric motors, and distribution systems into the aircraft's architecture [14, 15]. The Hybrid Mechatronic Actuation System, combining SHA and EMA, addresses the critical demands of reliability and safety in aircraft control. By mitigating common-mode and common-cause faults, the system significantly strengthens the actuation architecture, improving both robustness and operational efficiency [16].

While earlier research has contributed to the design of the Hybrid Mechatronic Actuation System (HAS), certain issues persist. SHA and EMA possess distinct mechanical structures, which result in different displacement and force responses despite receiving identical control signals from the pilot, owing to their fundamentally different actuation methods [17]. Rigid coupling of the EMA and SHA to the aircraft control surfaces introduces an intercoupling effect between the actuators. This effect, known as Force-Fighting, arises when both actuators exert forces on the surface at the same time. Force-Fighting refers to the difference in force outputs generated by two redundant actuators working simultaneously, which can degrade the control surface tracking performance and even risk physical damage [10]. To overcome the challenges of Force-Fighting, it is essential to design a controller that can effectively synchronize the movements of both actuators. Salman explored multiple control approaches in an attempt to resolve the Force-Fighting issue [18-22]. It has been found that proper synchronization is essential in controlling actuator movements to reduce the effects of Force-Fighting [23-25]. Ultimately, the development of synchronization controllers emerged as a primary focus within the aviation industry [26-28]. Force-Fighting must be mitigated to ensure that hybrid actuation systems produce synchronized output forces. The problem was resolved through a position demand offset, derived by incorporating both the measured actuator forces and the average force discrepancy into the integrator [29]. Research has also demonstrated methods for designing controllers for a Hybrid Mechatronic Actuation System (HAS), comprising EMA and SHA, capable of managing static forces [17, 30]. Improving the precision and accuracy of tracking control requires a controller design that addresses uncertainties, external disturbances, nonlinear behaviors, and the coupling effects between EMA and EHSA. Synchronizing the motions of multiple actuators operating in parallel has proven to be a highly effective solution for the Force-Fighting problem in hybrid mechatronic actuation systems [10]. Research by Rehman has explored multiple control methods aimed at synchronizing the motion of hybrid mechatronic actuation systems combining electrohydrostatic and servo-hydraulic actuators [31-35]. Wang explored the use of sensorless control strategies to coordinate motion in hybrid mechatronic actuation systems [36-38]. Research progress in hybrid mechatronic actuation systems enabled Cochoy and colleagues to develop a force equalization controller by utilizing

displacement, velocity, and force state feedback signals [11]. The ideal hypothesis suggests that a controller should account for all contributing signals, enabling the hybrid mechatronic actuation system to predict system motion. Since acquiring all state signals from an aircraft actuation system is challenging, a HAS test bench was developed with multiple sensors to obtain complete state information [13]. These methods, however, increase actuator weight and cost, limiting their broader applicability. This study presents a mathematical model of the Hybrid Mechatronic Actuation System and proposes an extended observer-based backstepping control strategy, which is then tested via MATLAB/Simulink simulations.

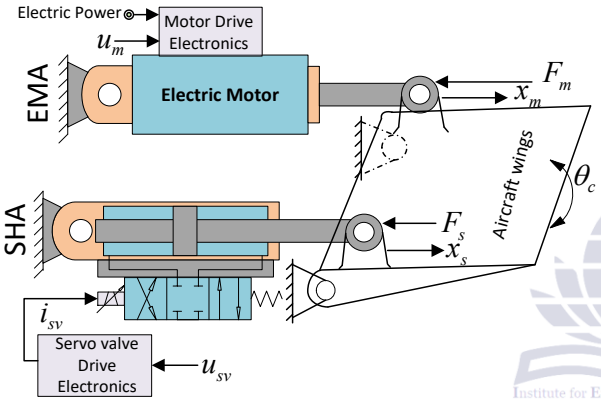

Figure 1 Development and Design of Hybrid Mechatronic Actuation Systems

2. Problem Statement

The key elements of a Hybrid Mechatronic Actuation System are the control surface, EMA, and SHA, shown in Figure 1. A Servo-Hydraulic Actuation System (SHA) is an electrically powered system that controls the flow and motion of hydraulic fluid to an actuator. Servo valves typically require only minimal electrical input to operate high-power hydraulic cylinders, allowing precise regulation of force, position, pressure, and velocity. They are also characterized by rapid response and effective damping properties.

An Electromechanical Actuator (EMA), on the other hand, converts electrical energy into mechanical force through an electric motor. The motor generates rotational motion, which is subsequently transformed into linear motion via a gear mechanism. In the Hybrid Mechatronic Actuation System (HAS), the SHA and EMA receive input control signals denoted as u_{sv} and u_m respectively, and are rigidly coupled to the aircraft's control surface. While the EMA uses an electric motor for actuation, the SHA relies on a servo valve.

Force-Fighting occurs when both actuators simultaneously exert force on the control surface, resulting from differences in their output forces. This phenomenon is primarily due to the SHA responding faster than the EMA, as the electric motor of the EMA exhibits a slower response time. Force-Fighting can be prevented if the actuators are coordinated such that each contributes equally to driving the control surface. Mathematically, this condition can be expressed as:

$$\text{Force Fighting} = F_{fight} = F_s - F_m \quad (1)$$

$$F_{fight} = F_s - F_m = k_s\left(x_s - x_c\right) - k_m\left(x_m - x_c\right) \quad (2)$$

$$F_{fight} = F_s - F_m = k\left(x_s - x_m\right) \qquad \therefore k_m = k_s = k \quad (3)$$

In this context, x_c represents the linear displacement of the aircraft's control surface, x_m denotes the motion of the Electromechanical Actuator (EMA), and x_s corresponds to the movement of the Servo-Hydraulic Actuator (SHA). F_m and F_s indicate the forces generated by the EMA and SHA, respectively. Equation (3) implies that Force-Fighting is avoided when the displacements of both actuators in a hybrid mechatronic actuation system are identical. Provided that the transmission stiffness of both actuators is also the same, the system will operate without undesired force conflicts

3. Hybrid Mechatronic Actuation System: Mathematical Formulation

Each element of the Hybrid Mechatronic Actuation System—including the control surface, Electromechanical Actuator (EMA), and Servo-Hydraulic Actuator (SHA)—will be modeled individually

3.1 Control Surface: Mathematical Representation

The motion of the aircraft's control surface follows Newtonian mechanics and is represented by the following equations:

$$\left(F_s + F_m\right) r_c = j_c \ddot{\theta}_c + F_{air} r_c \quad (4)$$

$$F_s = k_s\left(x_s - x_c\right) \quad (5)$$

$$F_m = k_m\left(x_m - x_c\right) \quad (6)$$

Here, k_s represents the transmission stiffness coefficient of the Servo-Hydraulic Actuator (SHA), k_m denotes the transmission stiffness coefficient of the Electromechanical Actuator (EMA), r_c is the radial distance, and j_c is the moment of inertia associated with the angular motion θ_c of the control surface. It has been observed that the angular displacement is relatively small. Under this condition, θ_c and x_c can be approximated as linear quantities [39], related through the following expression;

$$x_c = \theta_c r_c \quad (7)$$

3.2 Servo-Hydraulic Actuation System: Mathematical Representation

A servo valve actuator consists of a hydraulic cylinder, a servo valve, and several additional components. The servo valve is a highly effective device for regulating fluid flow and is commonly employed in applications that require motion control through hydraulic power [40, 41]. Prior work shows that the dynamics of the hydraulic cylinder and servo valve are represented as [17];

$$x_{sv} = k_{sv}u_{sv} \quad (8)$$

$$Q_{sv} = k_{sq}x_{sv} - k_{sc}p_f \quad (9)$$

Here, x_{sv} denotes the spool displacement of the servo valve, u_{sv} represents the input signal applied to the servo valve coil, k_{sq} is the flow gain relative to valve opening, and k_{sc} is the flow gain relative to pressure. The force and flow dynamics of the servo-hydraulic actuator can be expressed as follows [17, 42];

$$\begin{aligned} Q_{sv} &= A_j\dot{x}_s + \frac{v_j}{4E_j}\dot{p}_f + k_{ac}p_f \\ F_j &= m_j\ddot{x}_s + B_j\dot{x}_s + F_s \end{aligned} \quad (10)$$

Here, E_j represents the oil bulk modulus, v_j is the effective piston volume, A_j denotes the piston's operating area, p_f is the load pressure, k_{ac} is the leakage coefficient, $F_j = A_j p_f$ is the force generated by the actuator, B_j is the damping coefficient, and m_j is the piston mass

Let suppose the state vector of SHA can be defined as $x_1 = [x_{11}, x_{12}, x_{13}]^T = [x_s, \dot{x}_s, \ddot{x}_s]^T$. The state-space representation of the servo-hydraulic actuation system can then be expressed as follows:

$$\Omega_{SHA} = \begin{cases} \dot{x}_{11} = x_{12} \\ \dot{x}_{12} = x_{13} \\ \dot{x}_{13} = f_1\left(x_1\right) + g_1 + \sigma_1 u_1 \end{cases} \quad (11)$$

Where;

$$f_1\left(x_1\right) = -\frac{4E_j k_{hs}\left(k_s + k_{ac}\right)}{m_j v_j}x_{11} - \frac{4E_j A_j^2 + 4E_j B_j\left(k_s + k_{ac}\right) + v_j}{m_j v_j}x_{12} - \frac{4E_j m_j\left(k_s + k_{ac}\right) + B_j v_j}{m_j v_j}x_{13}$$

$$g_1 = \frac{4E_j k_{hs}\left(k_{sq} + k_{ac}\right)}{m_j v_j}x_c - \frac{k_{hs}}{m_j}\dot{x}_c$$

$$\sigma_1 = \frac{4A_j E_j k_{sq} k_{sv}}{m_j v_j}$$

3.3 Electromechanical Actuation System: Mathematical Representation

In an Electromechanical Actuator (EMA), the electrical dynamics of the electric motor are described by [13, 43];

$$u_m = k_m\omega_m + L_m\frac{di_m}{dt} + R_m i_m \quad (12)$$

$$T_m = k_{bm}i_m \quad (13)$$

The armature current i_m, inductance L_m, and resistance R_m characterize the electrical properties of the motor. The angular velocity is denoted by ω_m, while K_{bm} represents the back EMF constant and T_m the generated electromagnetic torque. This torque counterbalances the effects of damping and is subsequently transmitted to the system as inertial and load-driven dynamics.

$$T_m - T_L = j_m\frac{d\omega_m}{dt} + B_m\omega_m \quad (13)$$

The load torque T_L, damping coefficient B_m, and total inertia J_m characterize the system dynamics. The translational and rotational components are related through the following transmission equation:

$$\begin{cases} \dot{x}_m = \dfrac{1}{\eta_m k_{gm}}\omega_m \\ T_L = \dfrac{1}{\eta_m k_{gm}}F_m \end{cases} \quad (13)$$

Here, k_{gm} denotes the transmission coefficient, and η_m represents the transmission efficiency.

Assume State vector of EMA are $x_2 = [x_{21}, x_{22}, x_{23}]^T = [x_m, \dot{x}_m, \ddot{x}_m]^T$ and the control input for the electromechanical actuator is defined as $(u_2 = u_m)$. The state-space representation of the electromechanical actuator can be expressed as:

$$\Omega_{EMA} = \begin{cases} \dot{x}_{21} = x_{22} \\ \dot{x}_{22} = x_{23} \\ \dot{x}_{23} = f_2(x_2) + g_2 + \sigma_2 u_2 \end{cases} \quad (14)$$

Here;

$$f_2(x_2) = -\frac{R_m k_{ms}}{L_m j_m k_{gm}^2 \eta_m^2} x_{21} - \frac{k_{bm} k_m k_{gm}^2 \eta_m^2 + L_m k_{ms} + R_m B_m k_{gm}^2 \eta_m^2}{L_m j_m k_{gm}^2 \eta_m^2} x_{22} - \frac{B_m L_m + j_m R_m}{j_m L_m} x_{23}$$

$$g_2 = \frac{R_m k_{ms}}{L_m j_m k_{gm}^2 \eta_m^2} x_c + \frac{k_{ms}}{j_m k_{gm}^2 \eta_m^2} \dot{x}_c \quad , \quad \sigma_2 = \frac{k_{bm}}{L_m j_m k_{gm} \eta_m}$$

4. Extended State Observer-Driven Sliding Mode Control

The complete schematic of the proposed sliding mode motion synchronization controller, based on an extended state observer, is illustrated in Figure 2. The control strategy integrates an extended state observer, a sliding mode controller, a servo-hydraulic actuator, an electromechanical actuator, and a control surface. In the diagram, X_r denotes the reference pilot command signal; u_m and u_s are the control inputs for the actuators; K_m and K_s represent the stiffness of the actuator rods connecting the actuators to the control surface; F_m and F_s are the actuator-generated forces; F_{air} is the external force acting on the control surface; and x_m and x_s denote the actuator displacements.

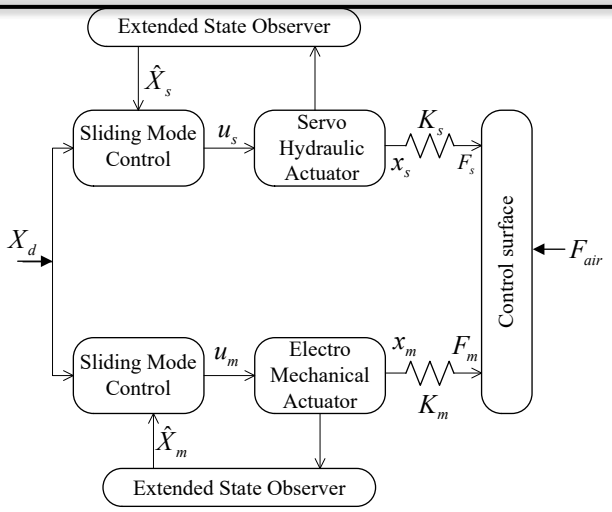

Figure 2 Block diagram of the mechatronics HAS

4.1 Sliding Mode Control:

Sliding Mode Control (SMC) represents a well-established robust control strategy, wherein the fundamental concept involves formulating an appropriate sliding surface that constrains the desired system trajectory. This control approach offers significant advantages, particularly its inherent insensitivity to parameter variations, modeling uncertainties, and external disturbances. Despite these strengths, SMC is often associated with the chattering phenomenon, which results from the high-frequency switching of control signals. To mitigate this undesirable effect, a commonly adopted solution involves replacing the discontinuous sign function with a continuous approximation, such as the saturation function, thereby achieving smoother control action. The sliding mode surface is given by;

$$s = \dot{e}_{i1} + \lambda e_{i1} \quad (15)$$

Where e_{i1} is tracking error which difference between between desired value or reference value and tracking value of displacement of air craft control surface. Mathematically is given by

$$e_{i1} = x_{i1} - x_d \quad \therefore i = 1 \Rightarrow SHA,\ i = 2 \Rightarrow EMA \quad (16)$$

Taking derivative of equation (15)

$$\dot{s} = \ddot{e}_{i1} + \lambda \dot{e}_{i1} \quad (17)$$

$$\ddot{s} = \dddot{e}_{i1} + \lambda \ddot{e}_{i1} = \dddot{x}_{i1} - \dddot{x}_d + \lambda \ddot{e}_{i1} \quad (18)$$

From equation (11) and (14)

$$\ddot{s} = f_i(x_i) + g_i + \sigma_i u_i - \dddot{x}_d + \lambda \ddot{e}_{i1} \quad \therefore \dddot{x}_{i1} = \dot{x}_{i3} \quad (19)$$

Where
$i=1\Rightarrow SHA$
$i=2\Rightarrow EMA$

Continuous control law that will acheieve $\ddot{s}=0$ is

$$u_i=\frac{1}{\sigma_i}\left(-f_i\left(x_i\right)-g_i+\ddot{x}_d-\lambda\ddot{e}_{i1}\right) \tag{20}$$

In order to acheieve robust performance despite disturbance on the system, we add $\hat{u}_i$ a saturation function across sliding mode surface

$$u_{ii}=u_i-Ksat\left(s/\phi\right) \tag{21}$$

Where K is chosen as a large constant to maintain system robustness, and ϕ characterizes the boundary layer thickness near the sliding mode surface.

If we look on equation (20) then there are nonlinearities and motion states of actuation system which are not easy to calculate let them represent with extended state.

$$x_{i4}=-f_i\left(x_i\right)-g_i \tag{22}$$

So there is need to design an observer which can calculate the value of this extended state x_{i4}. Consequently, a state observer is needed.

4.3 Extended State Observer

In this section, an extended state observer (ESO) is developed to estimate both the uncertainties and dynamic states of the electromechanical and servo-hydraulic actuators. The ESO considers all plant-influencing factors—including system nonlinearities, model uncertainties, and external disturbances—as a composite term, defined as the extended state, which is to be accurately estimated for enhanced control performance [44-46]. The incorporation of the extended state offers several advantages, including improved control performance, simplified implementation, and reduced dependence on the precise mathematical model of the plant.

Let suppose the state equation of actuator is given by;

$$\Omega_i:\begin{cases}\dot{x}_{i1}=x_{i2}\\ \dot{x}_{i2}=x_{i3}\\ \dot{x}_{i3}=x_{i4}+\sigma_i u_i & \therefore i=1\Rightarrow SHA\\ \dot{x}_{i4}=h_i & \therefore i=2\Rightarrow EMA\\ y_i=x_{i1}\end{cases} \tag{23}$$

Where h_i is variation rate of the uncertainty, and it is considered to be bounded.

Rewriting equation (23) in matrix form:

$$\begin{aligned}&\dot{X}_i=A_iX_i+B_iu_i+E_ih_i && \therefore i=1\Rightarrow SHA\\ &y_i=C_iX_i && \therefore i=2\Rightarrow EMA\end{aligned} \tag{24}$$

Where $A_i=\begin{bmatrix}0&1&0&0\\0&0&1&0\\0&0&0&1\\0&0&0&0\end{bmatrix}$, $B_i=\begin{bmatrix}0\\0\\\sigma_i\\0\end{bmatrix}$, $C_i=\begin{bmatrix}1\\0\\0\\0\end{bmatrix}$, $E_i=\begin{bmatrix}0\\0\\0\\1\end{bmatrix}$

Now, extended state observer for the system in (24), is given by;

$$\dot{\hat{X}}_i=A_i\hat{X}_i+B_iu_i+L_iC_i\left(X_i-\hat{X}_i\right) \quad \therefore i=1\Rightarrow SHA \quad \therefore i=2\Rightarrow EMA \tag{25}$$

Where $\hat{X}_i=\left[\hat{x}_{i1},\hat{x}_{i2},\hat{x}_{i3},\hat{x}_{i4}\right]$ $L_i=\left[\alpha_{i1},\alpha_{i2},\alpha_{i3},\alpha_{i4}\right]^T$ is state and designed vector for extended state observer. Observer gain can be found through pole placement, one typical example is

$$L_i=\left[4\omega_i,6\omega_i^2,4\omega_i^3,\omega_i^4\right]^T \tag{26}$$

Where ω_i is the extended state observer's tuning parameter, and it is observer's bandwidth.

5. Simulation Results and Discussion

The proposed control approach, based on an Extended State Observer integrated with a Sliding Mode Control, is assessed through simulations of a hybrid mechatronic actuation mechanism designed for large civil aircraft. The simulation environment is constructed in MATLAB/Simulink, and the associated parameters utilized in the model are presented in Table 1.

TABLE 1 PARAMETERS OF ACTUATION SYSTEMS

Actuation Parts	Parameters	Values
(SHA)	k_{sv}	3.04×10^{-4} m/A
	k_{sq}	2.7 m^2/s
	k_{sc}	1.75×10^{-11} $(m^3/s)Pa$
	A_j	1.1×10^{-3} m^2
	v_j	1.1×10^{-4} m^3
	m_j	25 Kg
	B_j	1×10^4 N.s/m
	E_j	8×10^8 Pa
	k_{ac}	1×10^{-11} $(m^3/s)Pa$
(EMA)	k_m	0.161 V/(rad/s)
	L_m	4.13×10^{-3} H
	R_m	0.54 Ω
	k_{bm}	0.64 Nm/A
	j_m	1.136×10^{-3}
	B_m	4×10^{-3} Kg. m^2
	k_{gm}	1.256×10^3
	η_m	0.9 rad/m
Control Surface	k_s, k_m	1×10^8 N/m
	r_{cs}	0.1 m
	j_{cs}	6.0 Kg. m^2

In addition, to provide a fair and comprehensive evaluation of the observer–based sliding mode strategy, its behavior is compared with three alternative control schemes, each tested under three distinct operating scenarios.

Estended State Observer Based Sliding Mode Control (ESO-SMC): The parameters for controller is $\lambda = 100$ and $K = 50$ The value for tunning parameter for observer is $\omega_1 = \omega_2 = 10000$.

PID Control: A conventional PID controller is employed for comparison purposes, with the following gain settings: for the Servo-Hydraulic Actuator (SHA), $K_{Ph} = 3.8$, $K_{Ih} = 20$, and $K_{Dh} = 0.1$and for the Electro-Mechanical Actuator (EMA), $K_{Pm} = 16$, $K_{Im} = 2$ and $K_{Dm} = 0.5$.

State difference feedback PID Control (SDF-PID): The State-Difference Feedback (SDF) control approach, as introduced by Cochoy et al. [11]. is also implemented for comparative analysis. This technique employs the same PID controller structure described in the preceding section, augmented with feedback terms based on the differences in displacement, velocity, and Force-Fighting. The corresponding feedback gains are selected as $K_{SDF-x} = 150$, $K_{SDF-v} = 10$, and $K_{SDF-F} = 2 \times 10^{-6}$.

5.1 Simulation Results Using a Step Input Command

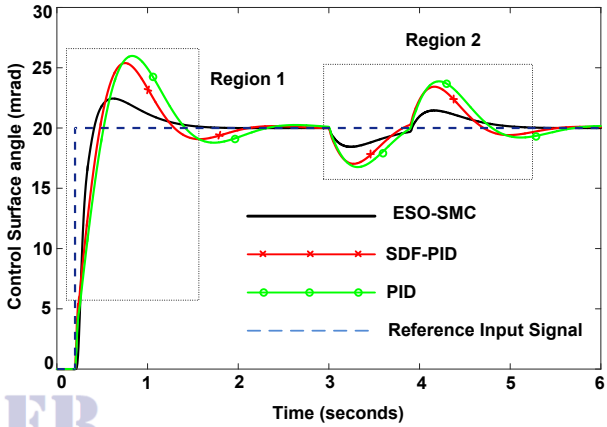

Figure 3 Motion Tracking Response under Step Input

As illustrated in Figure 3, the proposed ESO-SMC controller exhibits superior performance compared to the conventional PID and SDF-PID controllers in terms of both disturbance rejection and motion tracking accuracy. In Region 1, which represents the initial tracking phase without the influence of any external load, the ESO-SMC achieves the reference input more rapidly than other control methods. Moreover, the ESO-SMC response has less overshoot, whereas the PID and SDF-PID controllers display large overshoot accompanied by oscillations that require a considerable duration to settle. At approximately three seconds, a pulse load of 8 kN with a period of three seconds is applied to the aircraft control surface, introducing a jerk disturbance. The performance of the controllers under this condition, shown in Region 2, further demonstrates that the ESO-SMC provides markedly improved disturbance and load rejection capability compared to both SDF-PID and PID controllers. However, it is noteworthy that SDF-PID exhibits better disturbance rejection characteristics than the

conventional PID controller.

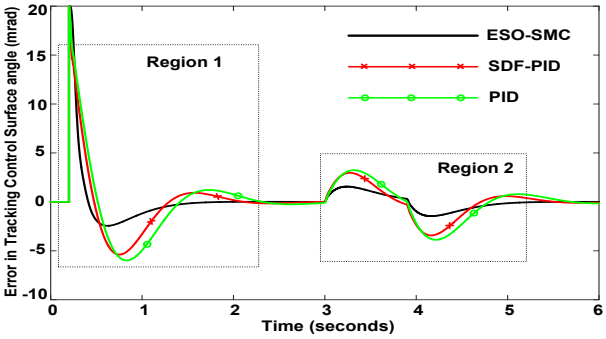

Figure 4 Error Analysis for Step Input

Figure 4 presents a comparative analysis based on tracking error. In Region 1, corresponding to the system's initial response to a step input, the ESO-SMC achieves a faster convergence rate and significantly lower tracking error relative to the SDF-PID and PID controllers. Even in Region 2, where an external load acts on the aircraft control surface, the tracking error for the ESO-SMC remains minimal. The phenomenon of Force-Fighting arises due to the disparity between the output forces of the two actuators—the Electro-Mechanical Actuator (EMA) and the Servo-Hydraulic Actuator (SHA)—which possess inherently different dynamic characteristics.

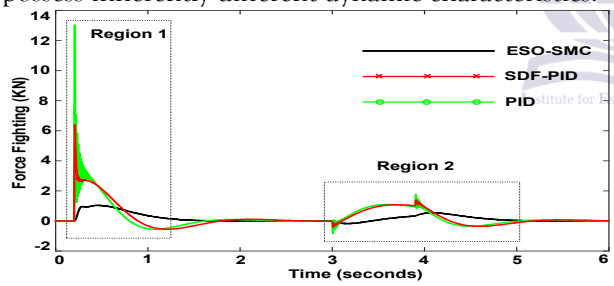

Figure 5 Force-Fighting Analysis under Step Input

Figure 5 illustrates this behavior, where Region 1 represents the initial Force-Fighting response. The observed Force-Fighting magnitudes are 13 kN for PID, 6.4 kN for SDF-PID, and only 1 kN for ESO-SMC, indicating that the proposed controller achieves the minimum Force-Fighting level. A similar trend is observed in Region 2, where the external pulse load is applied to the control surface, further validating the robustness of the ESO-SMC controller.

5.2 Simulation Results Using a Dynamic Input Command

Dynamic input signal simulations were also conducted to further evaluate the performance of the proposed control schemes.

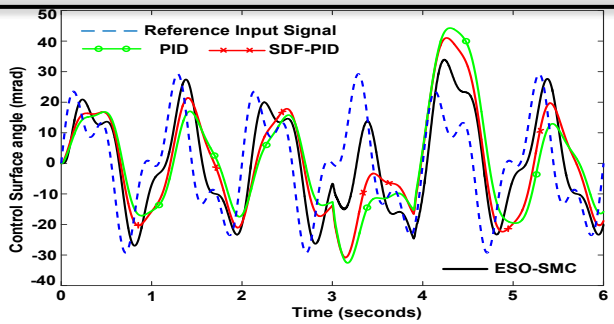

Figure 6 Motion Tracking Response under Dynamic Input

As illustrated in Figure 6, the ESO-SMC controller demonstrates markedly superior performance compared to both PID and SDF-PID controllers in terms of disturbance rejection and motion tracking response. Region 1 represents the initial tracking phase under no-load conditions. It can be observed that ESO-SMC achieves the reference trajectory more rapidly than the other controllers, exhibiting a faster response and reduced oscillatory behavior. At approximately three seconds, an external pulse load of 8 kN with a period of three seconds is applied to the aircraft control surface. The corresponding system behavior, represented in Region 2, reveals that ESO-SMC achieves superior load and disturbance rejection capability relative to the SDF-PID and PID controllers. Nevertheless, the SDF-PID shows improved disturbance rejection compared to the conventional PID control scheme.

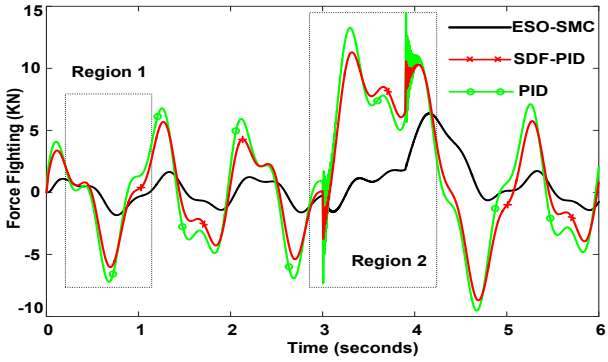

Figure 7 Force-Fighting Behavior under Dynamic input

Further analysis was performed with respect to Force-Fighting behavior, which is a critical factor in ensuring effective motion synchronization between actuators. The minimization of Force-Fighting is essential, as its presence hinders coordinated actuator motion. As depicted in Figure 7, Region 1 illustrates the initial Force-Fighting characteristics. The observed Force-Fighting magnitudes are approximately 4 kN for PID, 3 kN for SDF-PID, and only 0.5 kN for the

proposed ESO-SMC controller, indicating its superior capability in mitigating this phenomenon. The lowest Force-Fighting amplitude is therefore achieved by the ESO-SMC controller. A similar trend is observed in Region 2, where the external pulse load acts on the control surface, further confirming the robustness and efficiency of the proposed control strategy in handling dynamic and load-varying conditions.

5.3 Simulation Results Using a Real-Time Input Signal

Simulations were also conducted using a real-time input signal to further evaluate controller performance. As presented in Figure 8, the ESO-SMC controller demonstrates superior performance compared to conventional PID and SDF-PID controllers in terms of disturbance rejection and motion tracking accuracy. Region 1 represents the initial tracking phase under no-load conditions. It is evident that the ESO-SMC achieves the reference trajectory more rapidly and with improved tracking precision compared to PID and SDF-PID controllers. At (t = 3) s, an external pulse load of 8 kN with a period of 3 s is applied to the aircraft control surface. The response shown in Region 2 indicates that ESO-SMC exhibits enhanced load disturbance rejection capability. Although the SDF-PID controller performs better than the PID, its performance remains inferior to that of ESO-SMC.

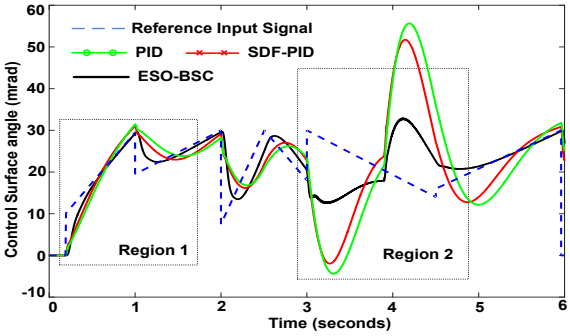

Figure 8 Motion Tracking Behavior with Real-Time Input

Further comparison was carried out with respect to Force-Fighting characteristics, which are critical for maintaining actuator motion synchronization.

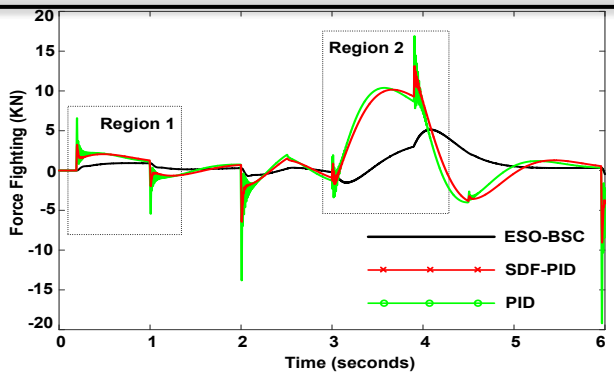

Figure 9 Force-Fighting Behavior under Real-Time Command and Pulse Load

Figure 9 illustrates the Force-Fighting response, where Region 1 corresponds to the initial condition. The observed Force-Fighting magnitudes are 6.2 kN for PID, 3 kN for SDF-PID, and only 0.5 kN for the proposed ESO-SMC controller, confirming its superior capability in minimizing inter-actuator force discrepancies. The lowest Force-Fighting amplitude is achieved by ESO-SMC. A similar response trend is observed in Region 2 when the external pulse load is applied, further validating the robustness and dynamic coordination performance of the proposed controller.

6. Conclusions

In conclusion, the extended state observer–based sliding mode control framework developed for the hybrid mechatronic actuation system has demonstrated improved performance in managing nonlinear coupling dynamics, uncertainties, and external disturbances while ensuring precise motion synchronization. The simulation results indicate a substantial reduction in force-fighting during both transient and steady-state conditions, even in the presence of aerodynamic disturbance loads. Further comparison under step, dynamic, and real-time pilot command inputs confirms that the proposed method provides superior robustness, smoother synchronization behavior, and enhanced disturbance rejection relative to previously published approaches. These findings validate the effectiveness of the proposed control strategy for hybrid actuation systems where precise coordination and disturbance resilience are critical.

Future research will focus on experimental validation using a hardware test bench to further assess real-world performance and implementation feasibility. Additionally, extending the control framework to incorporate adaptive or learning-based mechanisms

may enhance its ability to cope with time-varying system parameters and unknown nonlinearities. Finally, performance optimization concerning computational efficiency and real-time embedded deployment will be investigated to support its integration into next-generation hybrid actuator platforms.

Appendix I:

Notation

k_{sv}	*Gain Coefficient*
k_{sq}	*Flow /opening gain*
k_{sc}	*Flow / pressure gain*
A_j	*Area of Piston*
v_j	*Cylinder chamber volume*
m_j	*Piston mass, including chamber*
B_j	*Damping constant*
E_j	*Bulk modulus constant*
k_{ac}	*Coefficient of Leakage*
k_m	*Back emf constant*
L_m	*Armature Inductance*
R_m	*Armature resistance*
k_{bm}	*Electromagnetic coefficient*
j_m	*Total inertia of rotating parts*
B_m	*Damping coefficient*
k_{gm}	*Transmission coefficient*
η_m	*Transmission efficiency*
k_s, k_m	*Connection stiffness*
r_{cs}	*Control surface's radial distance*
j_{cs}	*Control surface's moment of inertia*

REFERENCES

[1] H. Benchaita and S. Ladaci, "Fractional adaptive SMC fault tolerant control against actuator failures for wing rock supervision," *Aerospace Science and Technology*, vol. 114, p. 106745, 2021.

[2] A. R. Ynineb and S. Ladaci, "MRAC adaptive control design for an F15 aircraft pitch angular motion using Dynamics Inversion and fractional-order filtering," *International Journal of Robotics and Control Systems*, vol. 2, pp. 240-252, 2022.

[3] C. Zhang, B. Chen, and X. Li, "Fuzzy Failure Modes, Effect and Criticality Analysis on Electromechanical Actuators," in *Actuators*, 2024, p. 510.

[4] Y. Wu, G. Ling, and Y. Shi, "Robust Trajectory Tracking Fault-Tolerant Control for Quadrotor UAVs Based on Adaptive Sliding Mode and Fault Estimation," *Computation*, vol. 13, p. 162, 2025.

[5] M. Karpenko, "Landing gear failures connected with high-pressure hoses and analysis of trends in aircraft technical problems," *Aviation*, vol. 26, pp. 145–152-145–152, 2022.

[6] B. Kirwan, "The Impact of Artificial Intelligence on Future Aviation Safety Culture," *Future Transportation*, vol. 4, pp. 349-379, 2024.

[7] Q. Haitao, F. Yongling, Q. Xiaoye, and L. Yan, "Architecture optimization of more electric aircraft actuation system," *Chinese Journal of Aeronautics*, vol. 24, pp. 506-513, 2011.

[8] P. Goupil, "AIRBUS state of the art and practices on FDI and FTC in flight control system," *Control Engineering Practice*, vol. 19, pp. 524-539, 2011.

[9] D. Van Den Bossche, "The A380 flight control electrohydrostatic actuators, achievements and lessons learnt," in *25th international congress of the aeronautical sciences*, 2006, pp. 1-8.

[10] C. Shi, X. Wang, S. Wang, J. Wang, and M. M. Tomovic, "Adaptive decoupling synchronous control of dissimilar redundant actuation system for large civil aircraft," *Aerospace Science and Technology*, vol. 47, pp. 114-124, 2015.

[11] O. Cochoy, S. Hanke, and U. B. Carl, "Concepts for position and load control for hybrid actuation in primary flight controls," *Aerospace Science and Technology*, vol. 11, pp. 194-201, 2007.

[12] J. Fu, J.-C. Maré, and Y. Fu, "Modelling and simulation of flight control electromechanical actuators with special focus on model architecting, multidisciplinary effects and power flows," *Chinese Journal of Aeronautics*, vol. 30, pp. 47-65, 2017.

[13] O. Cochoy, U. B. Carl, and F. Thielecke, "Integration and control of electromechanical and electrohydraulic actuators in a hybrid primary flight control architecture," in *International Conference on Recent Advances in Aerospace Actuation Systems and Components*, 2007, pp. 1-8.

[14] K. Emadi and M. Ehsani, "Aircraft power systems: technology, state of the art, and future

trends," *IEEE Aerospace and Electronic Systems Magazine*, vol. 15, pp. 28-32, 2000.

[15] R. Naayagi, "A review of more electric aircraft technology," in *2013 international conference on energy efficient technologies for sustainability*, 2013, pp. 750-753.

[16] J. Rosero, J. Ortega, E. Aldabas, and L. Romeral, "Moving towards a more electric aircraft," *IEEE Aerospace and Electronic Systems Magazine*, vol. 22, pp. 3-9, 2007.

[17] L. Wang and J.-C. Mare, "A force equalization controller for active/active redundant actuation system involving servo-hydraulic and electro-mechanical technologies," *Proceedings of the institution of mechanical engineers, Part G: Journal of aerospace engineering*, vol. 228, pp. 1768-1787, 2014.

[18] I. Salman, Y. Lin, and M. T. Hamayun, "Fractional order modeling and control of dissimilar redundant actuating system used in large passenger aircraft," *Chinese Journal of Aeronautics*, vol. 31, pp. 1141-1152, 2018.

[19] S. Ijaz, L. Yan, M. T. Hamayun, and C. Shi, "Active fault tolerant control scheme for aircraft with dissimilar redundant actuation system subject to hydraulic failure," *Journal of the Franklin Institute*, vol. 356, pp. 1302-1332, 2019.

[20] S. Ijaz, M. T. Hamayun, L. Yan, H. Ijaz, and C. Shi, "Adaptive fault tolerant control of dissimilar redundant actuation system of civil aircraft based on integral sliding mode control strategy," *Transactions of the Institute of Measurement and Control*, vol. 41, pp. 3756-3768, 2019.

[21] S. Ijaz, M. T. Hamayun, H. Anwaar, L. Yan, and M. K. Li, "LPV modeling and tracking control of dissimilar redundant actuation system for civil aircraft," *International Journal of Control, Automation and Systems*, vol. 17, pp. 705-715, 2019.

[22] S. Ijaz, L. Yan, M. T. Hamayun, W. M. Baig, and C. Shi, "An adaptive LPV integral sliding mode FTC of dissimilar redundant actuation system for civil aircraft," *IEEE Access*, vol. 6, pp. 65960-65973, 2018.

[23] G. Cieplok and K. Wójcik, "Conditions for self-synchronization of inertial vibrators of vibratory conveyors in general motion," *Journal of Theoretical and Applied Mechanics*, vol. 58, 2020.

[24] P. Fang, M. Zou, H. Peng, M. Du, G. Hu, and Y. Hou, "Spatial synchronization of unbalanced rotors excited with paralleled and counterrotating motors in a far resonance system," *Journal of Theoretical and Applied Mechanics*, vol. 57, 2019.

[25] W. Ur Rehman, X. Wang, Z. Hameed, and M. Y. Gul, "Motion Synchronization Control for a Large Civil Aircraft's Hybrid Actuation System Using Fuzzy Logic-Based Control Techniques," *Mathematics*, vol. 11, p. 1576, 2023.

[26] W. Du, Y. Luo, Y. Luo, and H. Mu, "A Simulation Study of an Electro-Hydraulic Load-Sensitive Variable Pressure Margin Diverter Synchronous Drive System with Time-Varying Load Resistance," *Processes*, vol. 12, p. 170, 2024.

[27] N. Khanh and N. Hung, "Synthesis of an Adaptive Controller for Movement Synchronization in a Multi-channel Steering System," in *2024 XXVII International Conference on Soft Computing and Measurements (SCM)*, 2024, pp. 99-102.

[28] C. C. Nguyen, T. T. Nguyen, T. T. C. Duong, T. M. Nguyen, H. T. T. Ngo, and L. Sun, "Real-Time Experiments for Decentralized Adaptive Synchronized Motion Control of a Closed-Kinematic Chain Mechanism Robot Manipulator," *Machines*, vol. 13, p. 652, 2025.

[29] G. Jacazio and L. Gastaldi, "Equalization techniques for dual redundant electro hydraulic servo actuators for flight control systems," *Fluid Power and motion control*, vol. 2008, pp. 543-557, 2008.

[30] H. Qi, J.-C. Mare, and Y. Fu, "Force equalization in hybrid actuation systems," in *7th International Conference on Fluid Power Transmission and Control, Hangzhou*, 2009, pp. 342-347.

[31] W. U. Rehman, S. Wang, X. Wang, L. Fan, and K. A. Shah, "Motion synchronization in a dual redundant HA/EHA system by using a hybrid integrated intelligent control design," *Chinese Journal of Aeronautics*, vol. 29, pp. 789-798, 2016.

[32] U. R. Waheed, S. Wang, X. Wang, and A. Kamran, "A position synchronization control for HA/EHA system," in *2015 International Conference on Fluid Power and Mechatronics (FPM)*, 2015, pp. 473-482.

[33] W. U. Rehman, H. Nawaz, S. Wang, X. Wang, Y. Luo, X. Yun, *et al.*, "Trajectory based motion synchronization in a dissimilar redundant actuation system for a large civil aircraft," in *2017 29th Chinese Control And Decision Conference (CCDC)*, 2017, pp. 5010-5015.

[34] W. U. Rehman, X. Wang, S. Wang, and I. Azhar, "Motion synchronization of HA/EHA system for a large civil aircraft by using adaptive control," in *2016 IEEE Chinese Guidance, Navigation and Control Conference (CGNCC)*, 2016, pp. 1486-1491.

[35] W. U. Rehman, S. Wang, X. Wang, C. Shi, C. Zhang, and M. Tomovic, "Adaptive control for motion synchronization of HA/EHA system by using modified MIT rule," in *2016 IEEE 11th Conference on Industrial Electronics and Applications (ICIEA)*, 2016, pp. 2196-2201.

[36] X. Wang, R. Liao, C. Shi, and S. Wang, "Linear extended state observer-based motion synchronization control for hybrid actuation system of more electric aircraft," *Sensors*, vol. 17, p. 2444, 2017.

[37] X. Wang, C. Shi, and S. Wang, "Extended state observer-based motion synchronisation control for hybrid actuation system of large civil aircraft," *International Journal of Systems Science*, vol. 48, pp. 2212-2222, 2017.

[38] W. Ur Rehman, X. Wang, Y. Cheng, H. Chai, Z. Hameed, X. Wang, *et al.*, "Motion synchronization for the SHA/EMA hybrid actuation system by using an optimization algorithm," *Automatika*, vol. 62, pp. 503-512, 2021.

[39] L. L. Guo, L. M. Yu, Y. Lu, and D. L. Fan, "Multi-mode switching control for HSA/EHA hybrid actuation system," in *Applied Mechanics and Materials*, 2014, pp. 1088-1093.

[40] W. U. Rehman, W. Khan, N. Ullah, M. S. Chowdhury, K. Techato, and M. Haneef, "Nonlinear Control of Hydrostatic Thrust Bearing Using Multivariable Optimization," *Mathematics*, vol. 9, p. 903, 2021.

[41] W. U. Rehman, X. Wang, Y. Cheng, Y. Chen, H. Shahzad, H. Chai, *et al.*, "Model-based design approach to improve performance characteristics of hydrostatic bearing using multivariable optimization," *Mathematics*, vol. 9, p. 388, 2021.

[42] S. Wang, M. Tomovic, and H. Liu, *Commercial Aircraft Hydraulic Systems: Shanghai Jiao Tong University Press Aerospace Series*: Academic Press, 2015.

[43] X. Wang and S. Wang, "Adaptive fuzzy robust control of PMSM with smooth inverse based dead-zone compensation," *International Journal of Control, Automation and Systems*, vol. 14, pp. 378-388, 2016.

[44] S. E. Talole, J. P. Kolhe, and S. B. Phadke, "Extended-state-observer-based control of flexible-joint system with experimental validation," *IEEE Transactions on Industrial Electronics*, vol. 57, pp. 1411-1419, 2009.

[45] S. Talole and S. Phadke, "Extended state observer based control of flexible joint system," in *2008 IEEE International Symposium on Industrial Electronics*, 2008, pp. 2514-2519.

[46] J. Yao, Z. Jiao, and D. Ma, "Adaptive robust control of DC motors with extended state observer," *IEEE transactions on industrial electronics*, vol. 61, pp. 3630-3637, 2013.